Comptes Rendus

Physique

Botond Tyukodi, Armand Barbot, Reinaldo García-García, Matthias Lerbinger, Sylvain Patinet and Damien Vandembroucq

Coarse-graining amorphous plasticity: impact of rejuvenation and disorder

From everyday glass to disordered solids / *Du verre quotidien aux solides désordonnés*

Coarse-graining amorphous plasticity: impact of rejuvenation and disorder

Transfert d'échelle en plasticité amorphe : effet du rajeunissement et du désordre

Botond Tyukodi [a]**, Armand Barbot** [b]**, Reinaldo García-García** [c]**, Matthias Lerbinger** [†, b]**, Sylvain Patinet** [b] **and Damien Vandembroucq** [*, b]

[a] Department of Physics, Babeş-Bolyai University, 400084 Cluj-Napoca, Romania

[b] PMMH, CNRS, ESPCI Paris, Sorbonne Université, Université de Paris, Université PSL, F-75005 Paris France

[c] Departamento de Física y Matemática Aplicada, Facultad de Ciencias, Universidad de Navarra, Pamplona 31008, Spain

E-mails: tyukodi.botond@gmail.com (B. Tyukodi), armand.barbot@espci.fr (A. Barbot), regarciag@unav.es (R. García-García), sylvain.patinet@espci.fr (S. Patinet), damien.vandembroucq@espci.fr (D. Vandembroucq)

Abstract. The coarse-graining of amorphous plasticity from the atomistic to the mesoscopic scale is studied in the framework of a simple scalar elasto-plastic model. Building on recent results obtained on the atomistic scale, we discuss the interest of a disordered landscape-informed threshold disorder to reproduce the physics of amorphous plasticity. We develop a rejuvenation scenario that reproduces quasi-quantitatively the evolution of the mean local yield stress and the localization behavior. We emphasize the crucial role of two dimensionless parameters: the relative strength of the yield stress disorder with respect to the typical stress drops associated with a plastic rearrangement, and the age parameter characterizing the relative stability of the initial glass with respect to the rejuvenated glass that emerges upon shear deformation.

Résumé. Le transfert de l'échelle atomique à l'échelle mesocopique est étudié pour la plasticité d'un matériau amorphe modèle. En nous s'appuyant sur des résultats récents obtenus à l'échelle atomistique, nous discutons de l'intérêt d'un désordre de seuils enrichi par la connaissance du paysage désordonné à l'échelle atomique pour reproduire la physique de la plasticité amorphe. Nous montrons que la prise en compte d'un scénario de rajeunissement nous permet de reproduire de manière quasi-quantitative l'évolution de la limite d'élasticité locale moyenne et le comportement de localisation. Nous soulignons le rôle crucial de deux paramètres sans dimension : la force relative du désordre de la limite d'élasticité par rapport aux chutes de contraintes typiques associées à un réarrangement plastique, et le paramètre d'âge caractérisant la stabilité relative du verre initial par rapport au verre rajeuni qui émerge lors de la déformation par cisaillement.

* Corresponding author.

† Deceased.

1. Introduction

The plastic deformation of glasses and amorphous solids is a complex phenomenon. Dependence of the mechanical behavior (e.g. brittle or ductile) on preparation, avalanches and shear-banding are among its classical hallmarks. These features come together with a cohort of other puzzling properties: aging or rejuvenation [1–4]; plasticity-induced anisotropy and Bauschinger effect [5–7]; memory effects under cyclic loading [8, 9].

The understanding of the mechanical properties of glasses and amorphous materials has thus motivated an increasing amount of studies in the last decades [10–13]. In the absence of crystalline structure and thus of dislocations, it has appeared in particular that plastic deformation in amorphous materials results from series of localized rearrangements of the amorphous structure, Shear Transformations (ST) [14,15] that interact through the surrounding elastic medium [16–18]. The associated complex mechanical behavior naturally involves a wide range of time and length scales [11].

In parallel to the increasing number of atomistic simulations developed to study and characterize these various features, the last decades have seen the development of over-simplified lattice elasto-plastic models operating at a mesoscopic scale (see the recent review of Nicolas et al. [19] and references therein). Relying on the coupling of local threshold dynamics and a long-range elastic interaction induced by the local plastic rearrangements of the amorphous structure, these models were able to reproduce most of the complexity of amorphous plasticity despite the drastic reduction of degrees of freedom. In the same spirit as the Ising-like models for magnetism or the shell models for fluid turbulence, one may consider that mesoscopic Elasto-Plastic Models (EPMs) belong to the class of models recently coined by J.-P. Bouchaud [20] as *metaphoric*. Such models do not attempt to describe reality precisely or necessarily rely on very plausible assumptions. Instead, they aim to illustrate non-trivial mechanisms, the scope of which goes much beyond the specifics of the model itself.

Conversely, mesoscopic EPMs can also be considered as an important step in the framework of multiscale modelling of amorphous plasticity, operating at an intermediate scale between atomistic simulations and constitutive models at continuous scale [21]. Such a multiscale strategy requires identifying the parameters to be transferred to the upper scale and the calibration between the microscopic and mesoscopic scales. Driven by the rapid development of new characterization techniques of local shear transformations [22–26], this difficult question of a quantitative connection between atomistic and mesoscopic scale has very recently been addressed in Refs. [27–32].

At first sight, a complete quantitative agreement between atomistic and mesoscopic scales may appear elusive since it requires an ever-increasing number of parameters. Although not perfect, the above-cited works impressively reproduce several key aspects of amorphous plasticity upon quasistatic or finite shear rate loading: stress-strain curves, flow curves, creep [29] but also some of the microscopic and macroscopic fluctuations, as well as non-trivial emergent behaviors such as the Bauschinger effect [27] or shear-banding in a contact problem involving surface defects and spatial inhomogeneity of the stress field [30].

Here we discuss coarse-graining in a slightly different spirit. Sticking to the most simple scalar version of a mesoscopic elastoplastic model, we highlight the importance of taking into

account the structure and evolution of the underlying disordered glassy landscape. In particular, we explore the rejuvenation scenario proposed in Ref. [4], which states that upon loading, the glass is gradually transformed through local rearrangements into a new glass state with plastic properties that are close to that of an inherent state of a supercooled liquid, close to the mode coupling transition.

Building on recent atomistic studies [4, 25] we try to understand how to reproduce the most salient features of AQS (Athermal Quasistatic) simulations in the framework of lattice models with the sole knowledge of the properties measured in the initial atomic configurations. In particular, from the success, limitations and also failures of the different hypotheses that can be developed within this approach, we try to get more insight into the structure and evolution of the model's Potential Energy Landscape (PEL) upon shearing.

In the following, we first summarize in Section 2 recent results of AQS simulations of a simple binary model glass [4, 24, 25]. In particular, we show the contrasting localization behavior depending on glass preparation and discuss the statistics of local plastic thresholds in the initial state. In Section 3 we give a short presentation of the mesoscopic EPM. In Section 4, we present our up-scaling strategy. In Sections 5 and 6 we present and discuss comparisons of atomistic and mesoscopic results obtained for a poorly annealed glass and a gradually quenched glass characterized by a shear-banding behavior. We finally discuss in Section 7 different perspectives about the coarse-graining of amorphous plasticity.

2. Atomistic simulations of model glasses

2.1. *Preparation*

Three different two-dimensional binary Lennard-Jones (LJ) model glasses obtained with contrasting thermal histories are considered. For each glass, 100 samples of 10000 atoms are prepared. Details about the atomistic models and the protocols of preparation can be found in Refs. [4, 25]. Periodic boundary conditions are applied to the simulation box. In the following, all the physical quantities are given in LJ units. The binary system is prepared in the liquid state (NVT ensemble) at high temperature, then cooled down and equilibrated to a supercooled liquid state at $T = T_p$. Then the supercooled liquid at parent temperature T_p is either instantaneously quenched by energy minimization or gradually quenched at a slow rate down to a low-temperature glassy state ($T \approx 0.03$) before it is also abruptly quenched by energy minimization.

A first class of glasses is obtained from the instant quench of a supercooled liquid equilibrated at $T_p = 0.38$. This temperature is close to the estimated temperature of the Mode Coupling Transition of our system $T_{MCT} = 0.373 \pm 0.01$ [4]. This glass, which we will refer to as MCT in the following, will be used as a proxy of the glass structure at Mode Coupling Transition.

A second class of glasses is synthesized from the instant quench of a supercooled liquid equilibrated at $T_p = 0.351$. This temperature is still significantly higher than the numerical temperature of glass transition, estimated at $T_G \approx 0.31$. This glass which we will refer to as ESL (for Equilibrated Supercooled Liquid), will be used as a typical poorly annealed glass.

A third class of glass is obtained from the gradual quench of a supercooled liquid equilibrated at $T_p = 0.351$ and slowly quenched throughout 10^6 LJ time units. This glass, which we will refer to as GQ (for Gradual Quench), will be used as a typical well-annealed glass. This statement is obviously to be considered in the context of conventional molecular dynamics, i.e. in the absence of accelerated equilibration procedures such as the ones based on the swap Monte Carlo algorithm [33].
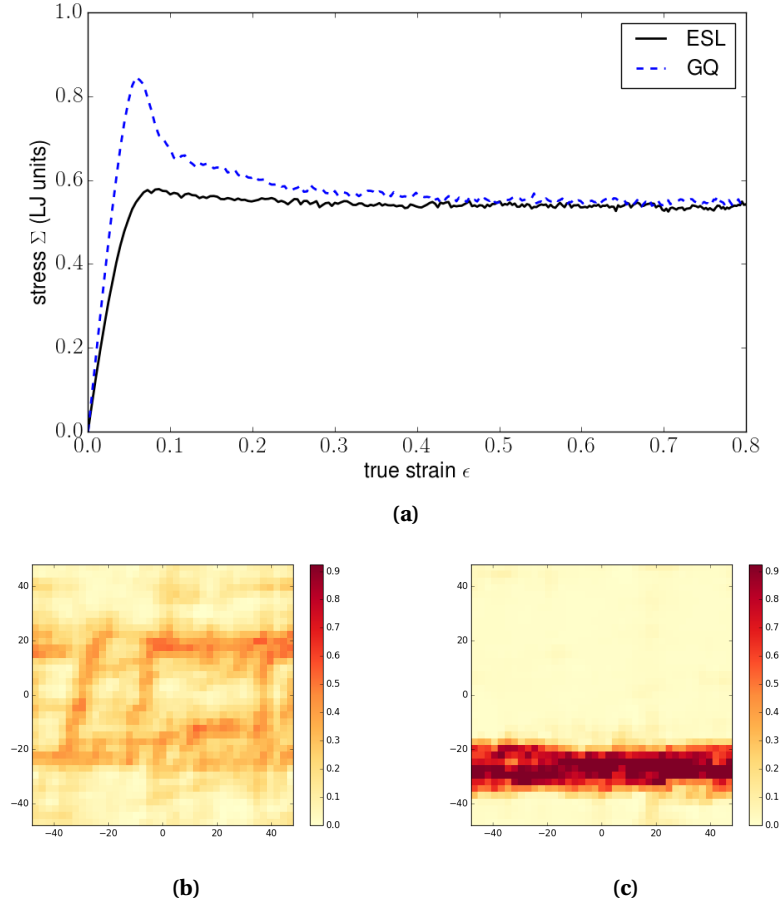
(a)

(b)   **(c)**

Figure 1. Plastic behavior obtained at atomistic scale for fast and slow quenched glasses
ESL and GQ respectively – **(a)** Stress-strain curves (after averaging over 20 realizations) –
Plastic strain field after 20% of total shear deformation in **(b)** the fast quenched glass ESL
and **(c)** the gradually quenched glass GQ. A shear band is clearly visible in the latter case.

2.2. *Athermal Quasistatic Shear loading*

The glass samples are deformed in simple shear geometry in AQS conditions, i.e. by series of
elementary deformation operations consisting of one small incremental affine global shear step
followed by an energy minimization step [34, 35]. The shearing protocol is applied up to a global
shear strain $\gamma = 5$. Local strain fields are computed by integration using Hencky's finite strain
definition. Details about the computation of the local stress and strain fields can be found in
Ref. [25].

In Figure 1 (a), we show the mean stress strain curves obtained for the soft glass ESL and the
hard gradually quenched glass GQ. While ESL shows a quasi-monotonic stress-strain curve, GQ
exhibits a stress peak followed by a softening branch. Eventually, independently of the initial
state, the two glasses reach the same stress plateau. In Figure 1 (b) and (c), we show strain
maps obtained after deforming ESL and GQ samples by 20%. While mild spatial fluctuations
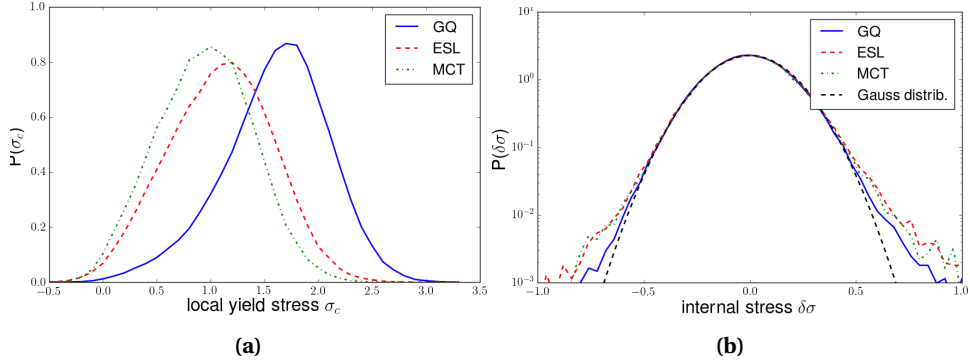are observed for ESL, a well-defined shear band is clearly visible for GQ.

Figure 2. Local Yield stress results: **(a)** distribution of local yield stress σ_c; **(b)** distribution of frozen stress fluctuations $\delta\sigma$.

2.3. *Local Yield Stress*

The propensity of the model glass for plastic deformation is estimated through the frozen matrix method exposed and detailed in Refs. [24,25]. A circular region of radius ξ is isolated in the model glass, with a surrounding shell of width $2R_c$, equal to twice the cut-off length of the interaction potential. The size $\xi = 5$ chosen for the radius of the inner core is such that continuum elasticity is obeyed but with significant fluctuations of the local moduli and anisotropy [36]. A series of affine steps of shear deformation is imposed on the (frozen) shell. After each step, only the inner core is allowed to relax. The deformation is incremented until a plastic event takes place in the core. The associated yield stress σ_c and stress drop $\Delta\sigma$ are computed. This operation is repeated in 18 different shearing directions regularly spaced every $10°$. Due to the heterogeneity of local elastic properties, the minimum stress to apply along a given direction to get a plastic rearrangement may be obtained for an affine deformation of the frozen outside shell in any other direction. The final local yield stress σ_c in the xy direction is thus defined as the (positive) minimum of the projected stress thresholds obtained in the 18 different directions [24].

We summarize below recent results obtained in Refs. [24, 25] on the small scale characterization of the plastic behavior of the three glasses (ESL, GQ, MCT) of interest. These results will help us to develop later our up-scaling strategy.

In Figure 2 (a), we show the distributions of local yield stresses $P(\sigma_c)$ for the three glasses ESL, GQ and MCT. As already documented in Refs. [4, 24, 25] we see clearly that the younger the glass, the lower the local yield stresses. In other terms, the frozen matrix method developed in Ref. [24] gives a microscopic interpretation of the relationship between the age and the mechanical stability of glasses. Note that a discrete negative tail is present in all three cases – this surprising feature results from the frozen stress field after the quench protocol. If we call $\delta\sigma(\mathbf{r})$ the internal shear stress in a patch located at $\mathbf{r}$ and $\sigma_c(\mathbf{r})$ its local yield stress, mechanical stability requires the satisfaction of the inequality $\delta\sigma(\mathbf{r}) < \sigma_c(\mathbf{r})$. We can thus define the local plastic strength $x(\mathbf{r}) = \sigma_c(\mathbf{r}) - \delta\sigma(\mathbf{r})$ which, contrary to the local yield stress has to remain positive to ensure mechanical stability. This local plastic strength is nothing but the amount of external shear stress to be applied so that the patch reaches its stability limit and experiences a plastic rearrangement.

In Figure 2 (b), we show the distributions of the local internal stress fields $\delta\sigma$ for the three glasses. Interestingly the three distributions fall onto the same Gaussian distribution of width $w_g = 0.175$. Despite the presence of a non-Gaussian tail for large fluctuations, the quench protocol thus does alter the frozen stress fields dramatically. These internal stress fluctuations in the initial configuration amount to about $10 - 20\%$ of the local yield stresses.

In Ref. [25], moreover, it was shown that the distribution $P(\Delta\sigma)$ of local stress drops $\Delta\sigma$ follows an exponential trend $P(\Delta\sigma) = \tau_{max}^{-1}\exp(-\Delta\sigma/\tau_{max})$ with the older the glass, the larger the local yield stress and the larger the value of τ_{max}. In addition, a parabolic dependence between the local stress drop and the local yield stress was reported: $\overline{\Delta\sigma} = a_0 + a_1\sigma_c^2$.

The frozen matrix method developed in Refs. [22, 24, 25] thus appears as a powerful tool to probe the disordered landscape of glassy material and its evolution upon loading. In the following, we use the new information collected through this method to inform the mesoscopic elastoplastic models.

3. A simple mesoscopic model of amorphous plasticity

Simulations at mesoscopic scale are performed using the scalar lattice model developed in Refs. [37–39]. We recall below the definition of the model and we highlight the crucial role of two dimensionless parameters associated with the amplitude of the elastic interaction and the evolution of the disorder upon loading, respectively.

3.1. *Basics of the scalar mesoscopic elastoplastic model*

Discretization – A spatial discretization is performed at scale a onto a square lattice of size $N \times N$. Bi-periodic boundary conditions are implemented. The material is considered as elastically homogeneous with a shear modulus μ and a compressive modulus K. In the following, we restrict ourselves to a scalar model and only consider the shear component of the stress tensor along the macroscopic shear loading direction. The mechanical state of a given configuration is then given by the shear stress field σ_{ij} and the plastic strain field ε_{ij}^p where (i, j) are the coordinates of the cell. The total strain field is thus the sum of the elastic and plastic strain fields: $\varepsilon_{ij} = \varepsilon_{ij}^{el} + \varepsilon_{ij}^p$ where by definition $\varepsilon_{ij}^{el} = \sigma_{ij}/2\mu$.

Local threshold dynamics – A local scalar criterion of plasticity is implemented: stability holds if $\sigma_{ij} < \sigma_{ij}^c$. Whenever the local stress exceeds the local thresholds, the cell experiences a small slip so that the local plastic strain is incremented by a small value $\delta\varepsilon_p$. The latter estimates the plastic strain experienced by a cell associated with a local rearrangement of the amorphous structure. The stress landscape of an individual cell thus consists of a series of elastic branches of slope 2μ terminating at a (fluctuating) threshold value along the stress scale and separated by (fluctuating) plastic strain increments along the strain scale. Note that here we focus on the mechanical behavior upon a monotonic shear loading. Therefore, we consider only stress thresholds in the forward direction and disregard thresholds in the backward direction.

Elastic interaction – Local plastic events take place in cells surrounded by other elastic cells. A local plastic strain ε_0 in an individual cell gives rise to a global plastic strain $\delta\varepsilon_{pl} = \varepsilon_0/N^2$. At constant total strain, this induces a decrease of the elastic strain of the same amount and thus a macroscopic stress drop $\delta\Sigma = 2\mu\varepsilon_0/N^2$. Moreover, it induces a local stress drop within the inclusion and a long-range internal stress field of quadrupolar symmetry in the far field. In the case of two-dimensional elasticity, we get for an Eshelby inclusion [40] of area $\mathscr{A} = \pi a^2$ experiencing an eigenstrain ε_0:

$$\Delta\sigma^{\text{in}}(r,\theta) = -\frac{\mu\varepsilon_0}{1 + \mu/K}, \tag{1}$$

$$\Delta\sigma^{\text{out}}(r,\theta) = \frac{\mu\varepsilon_0}{1 + \mu/K}\frac{\mathscr{A}\cos(4\theta)}{\pi r^2}. \tag{2}$$

where the superscripts *in* and *out* correspond to the inner and outer parts of the inclusion. Note that the local stress drop amplitude is directly proportional to the eigenstrain ε_0 and that of the far

field is proportional to the product $\mathscr{A}\varepsilon_0$ of the inclusion area and the eigenstrain. To account for bi-periodic boundary conditions, the Eshelby Green function G is implemented in the reciprocal space. Details and discussions about different methods of implementing this long-ranged elastic kernel can be found in Ref. [38, 39, 41].

Disorder – In the initial state, the plastic thresholds σ_{ij}^c are drawn from an *initial* random distribution $p_i(\sigma_c)$. The plastic slip is accompanied by a renewal of the threshold whenever a plastic event occurs in a cell. The new threshold is drawn from a *renewal* random distribution $p_r(\sigma_c)$. In the classical *disordered* scenario, defined by $p_r = p_i$ the very same distribution is used for the plastic thresholds of the initial state and the plastic thresholds obtained after rearrangements: the materials is left statistically unchanged after a rearrangement. In the *rejuvenation* scenario, the two distributions p_r and p_i are different. The rationale behind this hypothesis early discussed in Ref. [37] is that there is no particular reason that the glassy state obtained in the initial state after a particular thermal history be the same as the one obtained after a mechanically activated plastic event. In particular, this choice is expected to allow rejuvenation and impact shear-banding [1, 42, 43]. In the following, two model variants will be used depending on which rejuvenation or disordered scenario is chosen.

Elementary event - Everytime the plastic criterion is satisfied in a cell (i, j), the basic brick of the model thus performs the following sequence of three operations:

- The strain field is incremented by a local plastic slip $\delta\varepsilon_p$ drawn from a random distribution $q(\delta\varepsilon_p)$;
- The stress field is incremented by the internal stress field $\delta\sigma = G * \delta\varepsilon_p$ induced in the material by the local slip $\delta\varepsilon_p$.
- Finally the local plastic threshold σ_c^{ij} is replaced by a new random value drawn in a *renewal* distribution $p_r(\sigma_c)$.

Synchronous quasistatic dynamics – The elastoplastic behavior of an amorphous material consists of a series of elastic loading branches interspersed of stress drops. Starting from a stable configuration, the weakest site (i^*, j^*) is identified as the one that minimizes the plastic strength field $x_{ij} = \sigma_{ij}^c - \sigma_{ij}$. A plastic event is performed at (i^*, j^*). The elastic stress redistribution has then potentially destabilized a set of other cells. After identification, this set of unstable cells is updated synchronously [39]. Again, the series of plastic events may have destabilized other cells. The elementary steps i) identification of unstable sites and, ii) synchronous updates are repeated until the avalanche stops, and a stable configuration is recovered. The whole sequence is then repeated until a target macroscopic strain value is reached.

This series of operations thus defines a quasistatic driving in the very same spirit as AQS in atomistic simulations: a global homogeneous deformation is applied up to the first instability takes place. The first plastic event triggers a series of successive plastic events (an avalanche). The global level of deformation is thus kept constant up to the end of the avalanche. These two steps (loading until the end of the elastic branch and plastic avalanche) are repeated as long as desired [39].

3.2. *Two Dimensionless parameters*

Before addressing in the next section the implementation of our coarse-graining strategy, we briefly discuss the role of two dimensionless parameters associated with disorder strength and rejuvenation, respectively. The stationary regime is controlled solely by the disorder strength while the transient regime (e.g. stress peak) is futhermore dependent of the rejuvenation parameter.

Disorder strength – In analogy with depinning we can define a disorder strength s that balances the fluctuations of the local yield stress $\Delta\sigma^c$ with the stress drop $\Delta\sigma^{in}$ induced by a plastic event of amplitude ε_0:

$$s = \frac{\Delta\sigma_c^r}{\Delta\sigma^{in}} = \frac{\Delta\sigma_c^r}{\mu^*\varepsilon_0} , \tag{3}$$

where $\mu^* = \mu/(1 + \mu/K)$ is an effective shear modulus associated with the stress drop within a plastic inclusion.

In the depinning context, the disorder strength would control the transition between weak and strong pinning (see Ref. [44] for a discussion in the case of crack front propagation in a heterogeneous material). In particular, it controls the value of the effective toughness of the material (the depinning threshold).

In the present case of amorphous plasticity, the effect of this disorder strength is more subtle and is at least two-fold. Suppose one considers plastic deformation confined within a thin shear band along the shear direction. In that case, one recovers the standard case of a depinning line with a positive elastic restoration stress along the band. If instead, one considers a deformation in the entire system, we get an elastic stress interaction whose sign fluctuates depending on the polar angle, which can be regarded as mechanical noise far from the inclusion. In this context, as early discussed in Ref. [38] the disorder strength s both controls the value of the stationnary flow stress σ_F:

$$\frac{\sigma_F - \overline{\sigma_c^r}}{\overline{\sigma_c^r}} = f(s) , \tag{4}$$

and the diffusion properties upon deformation *via* the typical value of the strain associated with a plastic event ε_0

$$\delta\varepsilon_{pl}^2 = g(s)\varepsilon_{tot} . \tag{5}$$

where $\varepsilon_{tot} = \varepsilon_{el} + \varepsilon_p$ is the total strain.

Note that both the disorder strength parameter s and the reduced flow stress are defined with respect to the mean plastic threshold of the renewal distribution. Again, this parameter is intended here to control the stationary flow regime.

Rejuvenation/age parameter – As mentioned above, when dealing with the disorder landscape of the amorphous solids, we have to consider i) the distribution $p_i(\sigma_c)$ of local yield stresses σ_c^i in the initial configuration, which depends on the particular preparation protocol used to prepare the glass; ii) the renewal distribution $p_r(\sigma_c)$ of the new local yield stresses σ_c^r of the zones that rearranged. We define an age (or rejuvenation) parameter:

$$r = \frac{\overline{\sigma_c^i} - \overline{\sigma_c^r}}{\overline{\sigma_c^r}} \tag{6}$$

A positive value of r corresponds to an *aged* material that *rejuvenates* upon shear loading. Such positive age parameter values were shown to be associated with shear banding: the larger r, the thinner and the more persistent the shear band [37].

In the following, we restrict ourselves to two limit cases rather than performing a complete parametric study. In the first one, we use for the renewal distribution of local yield stress, the very same one as in the initial state. In the absence of rejuvenation, we thus keep $r = 0$. In the framework of this *disordered* scenario, the only expected evolution of the actual distribution of local plastic thresholds is the statistical hardening induced by the exhaustion of weak spots upon loading [4, 38, 45]. In the second case, we test the rejuvenation scenario proposed in Ref. [4], i.e. we use for the renewal distribution, the distribution of thresholds associated with an instant quench from a supercooled liquid at a temperature close to the mode coupling transition. We thus use the distribution of local yield stresses obtained for the glass coined as MCT in

Section 2. In this scenario, performing the numerical application from the data obtained for the distributions of local yield stress for the different glasses, we get for the age parameter:

$$r^{ESL} = \frac{\overline{\sigma_c^{ESL}} - \overline{\sigma_c^{MCT}}}{\overline{\sigma_c^{MCT}}} \approx 0.14 \tag{7}$$

$$r^{GQ} = \frac{\overline{\sigma_c^{GQ}} - \overline{\sigma_c^{MCT}}}{\overline{\sigma_c^{MCT}}} \approx 0.65 \tag{8}$$

4. Upscaling strategy

We discuss here how to connect the above-defined mesoscopic model with the atomistic simulations. We identify the parameters of the models from the results obtained at the atomic scale. We also try to make more explicit the (numerous) hypotheses associated with this upscaling operation that involves a drastic reduction of degrees of freedom. Finally, we list the observables that will be compared between the simulations operating at the atomic and mesoscopic scales.

Before going further, let us first emphasize an obvious statement: the present coarse-graining operation is intended to fail, the model being too simple and caricatural to expect a complete quantitative agreement. Still, it is interesting to study how this class of scalar models can cope with the phenomenology of amorphous plasticity. In the following, we discuss the various coarse-graining parameters we can extract from atomistic simulations.

4.1. *Coarse-graining parameters*

- Elastic properties – We use the mean shear and bulk moduli μ and K computed in the initial state. In particular, the spatial fluctuations of the elastic properties and their evolution upon deformation are disregarded.
- Coarse-graining length scale – In the atomistic simulations, the plastic properties are estimated in disks of radius $\xi = 5$. The systems under study have a linear size $L \approx 100$. Here we use for the mesh size of the lattice model $\ell = \xi\sqrt{\pi} \approx 8.86$, slightly larger than ξ such that the area of one cell coincides with the area of the disk $\mathscr{A} = \pi\xi^2$ used to estimate the plastic thresholds in atomistic simulations [24, 25]. The linear size of the box used to perform the atomistic simulations is thus about 11ℓ. In the following, most mesoscopic simulations are performed on small systems of size N=16.
- Distributions of plastic thresholds – The distributions $p_i(\tau^c)$ used to model the two glasses at mesoscopic scale in their as-quenched initial state are directly the ones computed from atomistic simulations using Refs. [24, 25]:

$$p_i^{Gl}(\sigma_c) = \mathscr{P}^{Gl}(\sigma_c), \tag{9}$$

where $\mathscr{P}$ stands for the distribution measured from atomistic simulations and the superscript $Gl = ESL, GQ$ refers to the glass considered.

In the *disordered* variant of the model, we assume that the distribution of plastic thresholds remains invariant under deformation. We thus use $p_r(\sigma_c) = p_i(\sigma_c)$ for the distributions of renewed plastic thresholds that characterize the glassy state obtained after a plastic rearrangement.

In the *rejuvenation* variant of the model, we account for a deformation-induced rejuvenation effect. More precisely, we assume that the glassy local structure obtained after a plastic rearrangement is specific, and a priori different from the as-quenched glass. We actually expect that this new glassy structure contributes to the gradual

formation of the stationary glass eventually obtained after large deformation. In that perspective, the distribution $p_r(\tau^c)$ of the new plastic thresholds should be independent of the initial condition. In the general case, it should rather depend on loading conditions (strain rate, temperature). Following the observation reported above, we assume in this glassy variant that the renewal distribution of thresholds is the same as the distribution of initial thresholds in a glass abruptly quenched from a temperature close to the mode coupling transition:

$$p_r^{Gl}(\sigma_c) = \mathscr{P}^{MCT}(\sigma_c) \,. \tag{10}$$

- Distributions of local slip increments – The amplitude of the slip increments directly controls the level of elastic interactions in the system and as such, the final value of the flow stress [38] or the broadening rate of shear-bands [37]. This coupling parameter [46] is thus crucial for the plastic properties of amorphous solids. The determination of the local slip events remains extremely challenging [47]. The successful mapping recently obtained by Albaret et al. [48] between the stress field measured in the atomistic simulations of amorphous silicon under shear and a sum of elementary Eshelby stress fields opens the way toward a quantitative analysis of these local events. In Section 1, where we summarized results presented in Ref. [25], the local slip amplitudes were estimated after the measurement of the local stress drops obtained after the relaxation of the local glassy structure following a plastic rearrangement. Local slip amplitudes were shown to follow a power law distribution bounded by an exponential cut-off and to be significantly correlated with the local yield stress.

  In most mesoscopic models of amorphous plasticity, slip increments are settled at a constant value or drawn from a random distribution, generally uncorrelated with the plastic thresholds. In contrast, models based on an energy landscape naturally introduce a strong correlation between local slips and thresholds. The direct relationship between the two quantities thus depends on the precise shape of the potential energy landscape chosen in the model [49, 50].

  Here, we consider for the slip increments an exponential distribution where we account for a direct dependence on the stress threshold:

$$p(\varepsilon_0|\sigma^c) = \frac{1}{\overline{\varepsilon_0}(\sigma_c)} \exp\left(-\frac{\varepsilon_0}{\overline{\varepsilon_0}(\sigma_c)}\right) \,, \tag{11}$$

  where the mean value of the slip increment obeys a parabolic dependence on the local yield stress:

$$\overline{\varepsilon_0}(\sigma_c) = c_0 + c_1\sigma_c^2 \,. \tag{12}$$

In the following, the coefficients c_0 and c_1 will be used as tuning parameters to reproduce two features of the stress-strain curves: the values of the maximum stress and the flow stress. In order to test the importance of the correlation between local stress drops and local yield stresses, we will also try to fit only the flow stress value by tuning the sole coefficient c_0, thus fixing the other coefficient $c_1 = 0$.

As detailed below, a systematic comparison will then be made between atomistic and mesoscopic results for different observables of interest: strain field, stress field and their fluctuations. Note again that most of the parameters are directly extracted from the initial configurations of the atomistic simulations. Thus, we are left with a very constrained problem, and we have to deal only with one or two fitting parameters to reproduce the results.

4.2. *Observables*

The extreme simplicity of the mesoscopic model obviously limits the extent of observables to be compared between atomistic and mesoscopic scales. In the following, we present the evolution of the stress and strain fields upon shearing, as well as the evolution of the local plastic properties.

In order to make the comparison as quantitative as possible, we compute averaged behaviors (mean values or mean profiles) as well as their fluctuating part. In addition to the stress and strain fields, we also pay special attention to the local yield stress fields. Note that a thorough analysis of sample to sample fluctuations (not discussed here) can be found in Ref. [27].

5. Deformation of a soft/fresh glass

We consider here the deformation of the soft glass ESL. As discussed in the previous section, we want to gradually enrich the description of the disordered landscape and test the importance of two hypotheses: a rejuvenation effect and the correlation between local thresholds and slip increments.

5.1. *Stress-strain curve*

In the most naïve version, the EPM considers neither correlation nor rejuvenation. We implement a distribution of plastic thresholds similar to the one measured by the local yield stress method for the glass ESL. When the plastic criterion is satisfied in a cell, the latter experiences a local slip. The slip amplitude is taken from an exponential distribution of width c_0. To account for a change in local structure, a new plastic threshold is drawn from the very same distribution as the initial one. Here c_0 is a tunable parameter. Its value $c_0 = 0.0626$ is adjusted so that the stress plateau of the stress-strain curves reproduces the results of the AQS atomistic simulation.

In a second version, rejuvenation is considered: when a site has slipped, the plastic threshold is renewed, but its value is now taken from a rejuvenated distribution. Following the scenario discussed in Ref. [4], we use the distribution of thresholds obtained for a glass instantly quenched (inherent structure) from a liquid equilibrated at $T = 0.38$, a temperature close to the Mode-Coupling transition. As in the previous case, the width c_0 of the distribution of slip increment is used as a tunable parameter with $c_0 = 0.0506$ to reproduce the level of the stress plateau of the stress-strain curve.

We show in Figure 3 the comparisons of the stress-strain curve obtained with atomistic and mesoscopic simulations for the two scenarios. In both cases, the stationary regime is nicely reproduced. In other words, the stress plateau can be reproduced with various distributions of local yield stresses. We see, however, that in the absence of correlation between local thresholds and slip increments (Figure 3 (a)), the mesoscopic models fail to reproduce the transient part of the stress-strain curve. In particular, while a discrete peak is observed in atomistic simulations, the stress-strain curve remains monotonic in the mesoscopic case. Adding rejuvenation slightly improves the results, but the one-parameter fit performed here to reproduce the stress plateau clearly is unable to reproduce the transient part of the plastic behavior.

In the presence of correlation between local thresholds and slip increments (Figure 3 (b)), we observe on the contrary that the mesoscopic simulations reproduce the atomistic stress-strain curve very nicely. Here two tunable parameters were used. The width $\overline{\varepsilon_0}$ of the exponential distribution used to generate a slip increment ε_0 after a threshold σ_c is given by $\overline{\varepsilon_0} = c_0 + c_1 \sigma_c^2$. The additional parameter c_1 thus quantifies the level of correlation. The pair of parameters (c_0, c_1) is tuned so that the mesoscopic stress-strain curve reproduces the level of the stress peak and that of the stress plateau. We observe that the full curve is nicely fitted. This close agreement

persists independently on whether the rejuvenation hypothesis is used or not. We get $(c_0, c_1) = (0.0304, 0.0216)$ in the absence of rejuvenation and $(c_0, c_1) = (0.0276, 0.0206)$ with rejuvenation. These first results thus tend to emphasize the importance of the underlying structure of the potential energy landscape (PEL). In order to reproduce the atomistic results, we need to consider a hierarchical-like structure of the PEL such that the deeper the well (the larger the threshold), the further the neighboring well (the larger the slip).

Interestingly, the additional coefficient c_1 does not significantly affect the flow stress. If one computes the averages value $\overline{\varepsilon_0} = c_0 + c_1 \sigma_c^2$, we get $\overline{\varepsilon_0} = 0.0634$ (no rejuvenation) and 0.0521 (rejuvenation) in the presence of correlations, i.e. very close to the values 0.0626 and 0.0506 obtained without correlation. Despite the additional complexity, the dimensionless parameter s, directly proportional to ε_0, thus fully controls the level of the plateau stress.
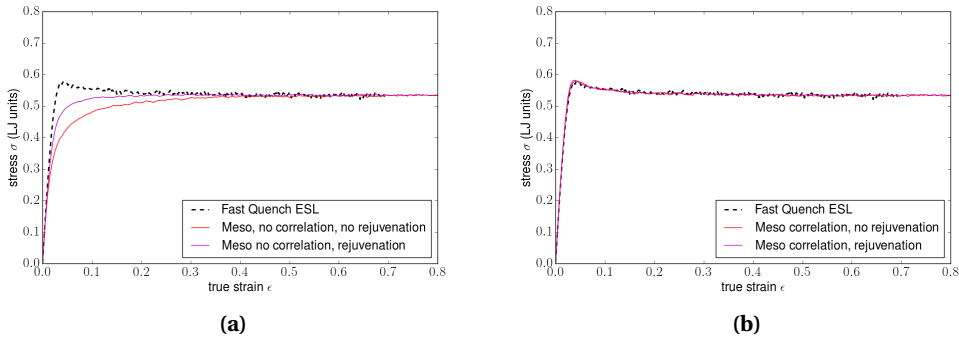

Figure 3. Stress-strain curves for the atomic glass ESL and a mesoscopic model without **(a)** and with **(b)** correlation between the characteristic slip increment and the stress threshold.
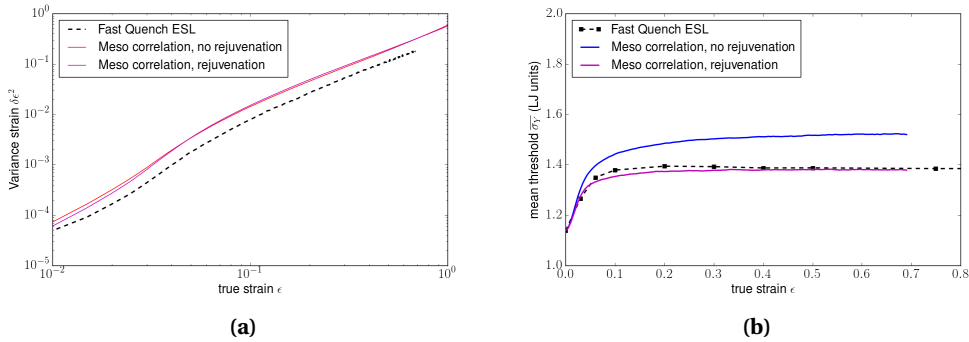

Figure 4. Variance of strain vs true strain **(a)** in the atomic glass ESL and the mesoscopic model **(b)**. Evolution of the mean threshold vs true strain in the atomic glass ESL and the mesoscopic model with and without rejuvenation.

5.2. *Strain fluctuations*

In Figure 4 (a), we show the evolution of the strain variance upon loading. Here we considered correlation between stress drops and local yield stress and used the coefficients (c_0, c_1) fitted

to reproduce the stress-strain curves with and without rejuvenation. We observe that, while the fluctuations obtained in the mesoscopic simulations overestimate the atomistic results by a factor of about 1.5, the global evolution of the variance upon loading is very nicely reproduced in the early and late regimes. We remark that the level of fluctuations apparently does not depend on the rejuvenation hypothesis: the curves almost superimpose. Again, as proposed in Ref. [38] this indicates that the diffusive behavior of the strain field is fully controlled by the sole disorder strength parameter *via* the typical value of the plastic slip $\overline{\varepsilon_0}$.

5.3. *Local yield stress*

In Figure 4 (b), we show the evolution of the local yield stresses upon loading. The atomistic results (dashed line with symbols) show a clear hardening trend. The average local yield stress shows an increase of about 10% upon loading. This increase takes place in the transient regime of deformation so that a stationary value is quickly reached. As for the strain fluctuation, we consider here the correlation case and study the effect of rejuvenation. Without rejuvenation, the mesoscopic model qualitatively reproduces the hardening trend but tends to overestimate the plastic thresholds. However, with rejuvenation, one observes a quasi-quantitative agreement with the atomistic results. In contrast to the plateau stress and the strain fluctuation, the reproduction of this observable crucially depends on the rejuvenation hypothesis. Accounting for the fact that the level of rejuvenation is not a free parameter but has been arbitrarily fixed by considering the renewal distribution as deriving from the glass MCT, this result gives a strong argument in support of the validity of the rejuvenation scenario.

6. Shear-banding of a hard/gradually quenched glass

We consider now the deformation of the hard gradually quenched glass GQ. As discussed in the previous section, we want to enrich the description of the disordered landscape gradually. We first focus on the respective effects of correlation and rejuvenation on the stress-strain curves. Since the latter exhibits a stress peak associated with a shear-banding behavior, we then follow the evolution of a localization ratio based on the participation ratio of the strain field. As for the fresh glasss ESL we also follow the evolution of the mean value of the local yield stress field.

6.1. *Stress-strain curve*

We show in Figure 5 the comparisons of the stress-strain curves obtained for the hard glass GQ with atomistic and mesoscopic simulations, respectively. As for the soft glass ESL, Figure 5 (a) shows the results in the absence of correlation between stress drop and local yield stress. In the absence of correlation and rejuvenation ($c_0 = 0.0836$), the plateau stress is correctly reproduced, but the only trace of a stress peak is a tiny bump. Conversely, in the presence of rejuvenation ($c_0 = 0.042$), even though the fitting procedure operates only on the stress plateau value, a well-defined stress peak gets clearly visible and almost reaches the atomistic value. The general shape of the stress-strain curve shows, however, evident discrepancies compared to atomistic data.

The results get better when accounting for the correlation between stress drops and local yield stresses and performing a two-coefficient fitting procedure. As required, both the values of the plateau stress and the stress peak are nicely reproduced. Without rejuvenation, we get $(c_0, c1) = (0.0344, 0.0164)$ and an excellent agreement in the stress-strain curve. In the presence of rejuvenation, we get $(c_0, c1) = (0.0235, 0.0163)$. Interestingly, the global reproduction of the stress-strain curve is not so good in this case, with a stress peak significantly sharper than in the atomistic case.
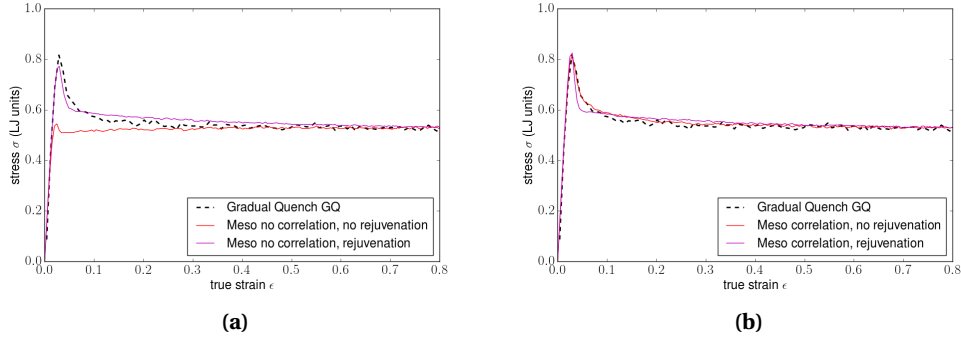
Figure 5. Stress-strain curve in the GQ and in the mesoscopic model **(a)** without and **(b)** with correlation between local stress drops and yield stress.

This discrepancy can have several causes. Let us mention two of them. First, due to the scalar nature of the model, there is one and only one slip direction. This implies a strong anisotropy of the internal stress field due to the repetitive addition of the same Eshelby quadrupolar elastic interaction. Second, the model is memoryless: the degree of plastic threshold renewal does not depend on the amplitude of the plastic event and a small slip can trigger a large weakening effect. As shown very recently in [31], the introduction of several slip directions (tensor model) and a memory scheme significantly improves the agreement between atomistic and mesocopic simulations.

As for the fresh glass ESL we note that the mean value of the slip increment $\overline{\varepsilon_0}$ keeps almost constant with and without correlation. Without rejuvenation we get $\overline{\varepsilon_0} = c_0 + c_1 \sigma_c^2 = 0.0833$ and with rejuvenation $\overline{\varepsilon_0} = 0.0429$. Again, these values are extremely close to those obtained above in the absence of correlation (0.0836 and 0.042). This confirms that the stress plateau level is fully controlled by the dimensionless parameter s (disorder strength) which is proportional to $\overline{\varepsilon_0}$.

6.2. *Localization*

In Figure 6 (a), we show the evolution of a localization index *LOC* of the strain field upon shear loading. This index is based on the participation ratio *PR* classically used to characterize localization phenomena. In practice, for a strain field ε_{ij} on a grid of linear size N, we define:

$$LOC(\varepsilon) = \frac{1}{N.PR(\varepsilon)} = \frac{N\sum_{ij} \varepsilon_{ij}^4}{\left(\sum_{ij} \varepsilon_{ij}^2\right)^2}. \tag{13}$$

In the case of localization of a single band, we get $LOC(\varepsilon) = 1$, while for a fully homogeneous field, we get $LOC(\varepsilon) = 1/N$. The glass GQ shows a strong localization behavior. The maximum value is obtained just after the stress peak and corresponds to the nucleation of a shear band. The subsequent broadening of the band then induces a gradual decrease in the localization index.

We compare these results with mesoscopic simulations performed with correlation of stress drops with local yield stresses and we discuss the effect of the rejuvenation hypothesis. The localization behavior appears to be very well reproduced by the mesoscopic model with rejuvenation and correlation. The global trend is recovered: a rapid increase associated with the nucleation of the band, followed by a slower decrease associated with the broadening of the band. The maximum value of the localization index is reasonably reproduced.
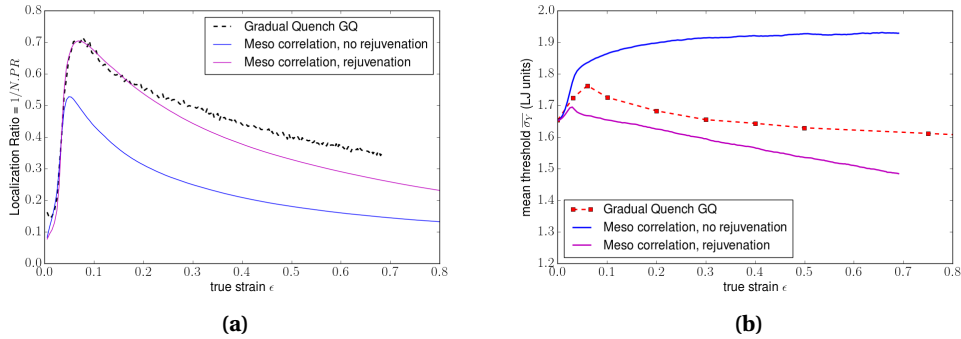
Figure 6. Evolution of **(a)** the localization ratio and of **(b)** the mean threshold vs true strain in the GQ glass and in the meso model with and without rejuvenation.

Note that even without rejuvenation, we still get a significant localization behavior. The global trend is recovered but the level of localization remains under-estimated.

6.3. *Local yield stress*

In Figure 6(b), we show the evolution of the mean value of the local yield stress upon shear deformation. As discussed in Ref. [4], a rather complex behavior emerges. We first observe a slight increase in the mean plastic threshold that can be associated with a statistical hardening process. Then a shear-band nucleates and broadens. The associated replacement of the old hard glass by a fresh softer one induces a gradual decrease in the average local yield stress.

We compare these atomistic results with the mesoscopic ones obtained with and without rejuvenation. Without rejuvenation, there is actually no mechanism at play that could tend to decrease the mean local yield stress. We thus only observe a growing trend which results from the statistical hardening discussed in Section 5 in the case of the glass ESL and the mesoscopic model significantly overestimates the values of the atomistic mean yield stress.

When accounting for rejuvenation, the mesoscopic results get better. In particular, we recover a similar trend as with the atomistic simulations: a first increasing regime, followed by a slow decreasing regime. However, from the quantitative aspect, the agreement is not spectacular and the mesoscopic model tends here to slightly underestimate the atomistic results. Still, it clearly appears here that the rejuvenation hypothesis is crucial to recover at least qualitatively the complex evolution of the mean yield stress upon loading.

7. Discussion

In this contribution, we discussed the coarse-graining of amorphous plasticity from the atomistic to the mesoscopic scale. We deliberately restricted ourselves to a very simplistic scalar version of a mesoscopic elasto-plastic model. We tried to identify a few key parameters of the underlying glassy landscape from the failures and successes encountered in this approach. In particular, we tried to test the rejuvenation scenario proposed in Ref. [4].

We emphasized the role of two dimensionless parameters, respectively associated with the strength of the disorder with respect to the typical stress drop and with the relative age of the initial glass with respect to the fresher one that emerges upon loading.

Testing our approach on two glasses of contrasting soft and hard behaviors, we could nicely reproduce the stress-strain curves, the evolution of the mean plastic thresholds and the localization behavior. We also got a qualitative agreement for the diffusive behavior of the strain field of the glass ESL.

7.1. *Structure of the disordered yield stress landscape*

The results we obtain are consistent with the rejuvenation scenario proposed in Ref. [4] according to which, upon shear deformation, the initial glass is gradually replaced by a fresh new one whose mechanical properties are close to a glass abruptly quenched from a temperature close to the mode coupling transition. We also made evidence for the necessity of correlating the local stress drops following a local plastic event with the height of the stress barrier, i.e. the local yield stress [25]. Such a relation is not unexpected and directly derives from the structure of the underlying potential energy landscape. Still, it is interesting to show that accounting for such a correlation between local stress drop and yield stress is necessary to reach a quantitative agreement between atomistic and mesoscopic simulations [27]. Additional features of the disordered yield stress landscape certainly deserve further study. In particular, we did not consider any memory. In the present implementation of the model, once a plastic event takes place, the former yield stress is immediately forgotten, independently of the amplitude of the local re-arrangement. This memory effect and its dependence on the initial preparation has been recently discussed in Ref. [31].

7.2. *Elastic heterogeneity and internal stress fluctuations*

In the present version of the mesoscopic model, elastic properties are homogeneous and do not evolve upon deformation. This assumption is at odds with the actual behavior observed in atomistic simulations. The macroscopic moduli significantly change upon shearing. In the stationary state, obtained after extensive deformation, one gets for the model glasses under study $\mu_{ss} = 13.2$ and $K_{ss} = 59$ to contrast with the initial values $\mu_{ESL} = 14.7$, $K_{ESL} = 52$ and $\mu_{GQ} = 19$, $K_{GQ} = 55$. These are significant changes, up to a few tens of per cent for the glass GQ.

The spatial heterogeneity of the elastic properties was also completely neglected in the present study. From the qualitative point of view, this omission may not be dramatic since the structure and the symmetry of the associated internal stress fields are likely to be close to those of the Eshelby stresses induced by plastic inclusions. From the quantitative point of view, the impact may be more significant.

Along with the relative (and sometimes impressive) success of the coarse-graining attempts reported so far in the present manuscript, it is essential to insist on the apparent failure that can be identified. In Figure 4, we reported strain fluctuations that overestimated the atomistic results by a factor of about 1.5. This overestimating trend of the microscopic fluctuations is all the more impressive when we focus on the internal stress field. In Figure 7, we report the evolution of the standard deviation of the internal stress fields for the ESL and GQ glasses and the associated mesoscopic models. While the latter does not account for the stresses induced by the elastic disorder, they overestimate the fluctuations by a factor 2 to 3. The reasons behind this large discrepancy are not entirely clear at this stage. The scalar character of the model may induce an effect of "constructive interference", artificially enhancing fluctuation that would be partly smeared out by an orientational disorder of the weak slip directions (see Refs. [27, 31] for discussion of the effect of full tensorial disorder). Another source of discrepancy may be the overestimation of the local yield stress by the frozen matrix method. In the same spirit, the mesoscopic model relies on a hypothesis of continuum elasticity in the rearranging regions
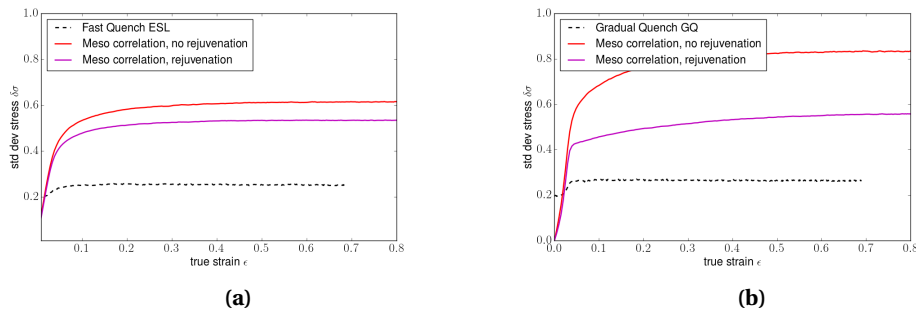
Figure 7. Evolution of the standard deviation of the internal stress field in the glasses **(a)** ESL and **(b)** GQ vs meso model.

and disregards non-affine elastic effects. The impact of these different points on internal stress fluctuations certainly deserves further study.

8. Acknowledgements

References

[1] M. Utz, P. G. Debenedetti, F. H. Stillinger, "Atomistic Simulations of Aging and Rejuveneation in Glasses", *Phys. Rev. Lett.* **84** (2000), p. 1471-1474.

[2] Y. Fan, T. Iwashita, T. Egami, "Energy landscape-driven non-equilibrium evolution of inherent structure in disordered material", *Nat. Commun.* **8** (2017), article no. 15417.

[3] Y. Tong, W. Dmowski, H. Bei, Y. Yokoyama, T. Egami, "Mechanical rejuvenation in bulk metallic glass induced by thermo-mechanical creep", *Acta Mater.* **148** (2018), p. 384-390.

[4] A. Barbot, M. Lerbinger, A. Lemaître, D. Vandembroucq, S. Patinet, "Rejuvenation and shear banding in model amorphous solids", *Phys. Rev. E* **101** (2020), no. 3, article no. 033001.

[5] C. L. Rountree, D. Vandembroucq, M. Talamali, E. Bouchaud, S. Roux, "Plasticity-induced structural anisotropy of silica glass", *Phys. Rev. Lett.* **102** (2009), article no. 195501.

[6] S. Karmakar, E. Lerner, I. Procaccia, "Plasticity-induced anisotropy in amorphous solids: The Bauschinger effect", *Phys. Rev. Lett.* **82** (2010), article no. 026104.

[7] S. Patinet, A. Barbot, M. Lerbinger, D. Vandembroucq, A. Lemaître, "Origin of the Bauschinger Effect in Amorphous Solids", *Phys. Rev. Lett.* **124** (2020), article no. 205503.

[8] D. Fiocco, G. Foffi, S. Sastry, "Encoding of Memory in Sheared Amorphous Solids", *Phys. Rev. Lett.* **112** (2014), no. 2, article no. 025702.

[9] N. C. Keim, J. D. Paulsen, Z. Zeravcic, S. Sastry, S. R. Nagel, "Memory formation in matter", *Rev. Mod. Phys.* **91** (2019), no. 3, article no. 035002.

[10] C. A. Schuh, T. C. Hufnagel, U. Ramamurty, "Mechanical behavior of amorphous alloys", *Acta Mater.* **55** (2007), p. 4067-4109.

[11] D. Rodney, A. Tanguy, D. Vandembroucq, "Modeling the mechanics of amorphous solids at different length and time scales", *Model. Simul. Mat. Sci. Eng.* **19** (2011), article no. 083001.

[12] D. Bonn, M. M. Denn, L. Berthier, T. Divoux, S. Manneville, "Yield stress materials in soft condensed matter", *Rev. Mod. Phys.* **89** (2017), article no. 035005.

[13] A. Tanguy, "Elasto-plastic behavior of amorphous materials: a brief review", *C. R. Physique* **22** (2021), p. 117-133.

[14] A. S. Argon, "Plastic deformation in metallic glasses", *Acta Metall.* **27** (1979), p. 47-58.

[15] M. L. Falk, J. S. Langer, "Dynamics of viscoplastic deformation of amorphous solids", *Phys. Rev. E* **57** (1998), p. 7192-7205.

[16] V. V. Bulatov, A. S. Argon, "A stochastic model for continuum elasto-plastic behavior. I. Numerical approach and strain localization", *Model. Simul. Mat. Sci. Eng.* **2** (1994), p. 167-184.

[17] V. V. Bulatov, A. S. Argon, "A stochastic model for continuum elasto-plastic behavior. II. a study of the glass transition and structural relaxation", *Model. Simul. Mat. Sci. Eng.* **2** (1994), p. 185-202.

[18] V. V. Bulatov, A. S. Argon, "A stochastic model for continuum elasto-plastic behavior. III. Plasticity in ordered versus disordered solids", *Model. Simul. Mat. Sci. Eng.* **2** (1994), p. 203-222.

[19] A. Nicolas, E. Ferrero, K. Martens, J.-L. Barrat, "Deformation and flow of amorphous solids: a review of mesoscale elastoplastic models", *Rev. Mod. Phys.* **90** (2018), article no. 045006.

[20] J. P. Bouchaud, "Econophysics: Still fringes after 30 years", *Europhys. News* **50** (2019), p. 24-27.

[21] E. van der Giessen, P. A. Schultz, N. Bertin, V. V. Bulatov, W. Cai, G. Csányi, S. M. Foiles, M. G. D. Geers, C. González, M. Hütter, W. K. Kim, D. M. Kochmann, J. LLorca, A. E. Mattsson, J. Rottler, A. Shlugera, R. B. Sills, I. Steinbach, A. Strachan, E. B. Tadmor, "Roadmap on multiscale materials modeling", *Model. Simul. Mat. Sci. Eng.* **28** (2020), article no. 043001.

[22] F. Puosi, J. Olivier, K. Martens, "Probing relevant ingredients in mean-field approaches for the athermal rheology of yield stress materials", *Soft Matter* **11** (2015), p. 7639-7647.

[23] T. Albaret, A. Tanguy, F. Boioli, D. Rodney, "Mapping between atomistic simulations and Eshelby inclusions in the shear deformation of an amorphous silicon model", *Phys. Rev. E* **93** (2016), article no. 053002.

[24] S. Patinet, D. Vandembroucq, M. L. Falk, "Connecting Local Yield Stresses with Plastic Activity in Amorphous Solids", *Phys. Rev. Lett.* **117** (2016), article no. 045501.

[25] A. Barbot, M. Lerbinger, A. Hernandez-Garcia, R. García-García, M. L. Falk, D. Vandembroucq, S. Patinet, "Local yield stress statistics in model amorphous solids", *Phys. Rev. E* **97** (2018), no. 3, article no. 033001.

[26] D. Richard, M. Ozawa, S. Patinet, E. Stanifer, B. Shang, S. A. Ridout, B. Xu, G. Zhang, P. K. Morse, J.-L. Barrat, L. Berthier, M. L. Falk, P. Guan, A. J. Liu, K. Martens, S. Sastry, D. Vandembroucq, E. Lerner, M. L. Manning, "Predicting plasticity in disordered solids from structural indicators", *Phys. Rev. Mater.* **4** (2020), article no. 113609.

[27] D. Fernández Castellanos, S. Roux, S. Patinet, "Insights from the quantitative calibration of an elasto-plastic model from a Lennard-Jones atomic glass", *C. R. Physique* **22** (2021), p. 135-162.

[28] F. Van Loock, L. Brassart, T. Pardoen, "Implementation and calibration of a mesoscale model for amorphous plasticity based on shear transformation dynamics", *Int. J. Plast.* **145** (2022), article no. 104079.

[29] C. Liu, S. Dutta, P. Chaudhuri, K. Martens, "Elastoplastic Approach Based on Microscopic Insights for the Steady State and Transient Dynamics of Sheared Disordered Solids", *Phys. Rev. Lett.* **126** (2021), article no. 138005.

[30] A. Tanguy, P. Chen, T. Chaise, D. Nélias, "Shear Banding in a Contact Problem between Metallic Glasses", *Metals* **11** (2021), article no. 257.

[31] D. Fernández Castellanos, S. Roux, S. Patinet, "History Dependent Plasticity of Glass: A Mapping between Atomistic and Elasto-Plastic Models", *Acta Mater.* **241** (2022), article no. 118405.

[32] G. Zhang, H. Xiao, E. Yang, R. J. S. Ivancic, S. A. Ridout, R. A. Riggleman, D. J. Durian, A. J. Liu, "Structuro-elasto-plasticity model for large deformation of disordered solids", *Phys. Rev. Res.* **4** (2022), article no. 043026.

[33] L. Berthier, E. Flenner, C. J. Fullerton, C. Scalliet, M. Singh, "Efficient swap algorithms for molecular dynamics simulations of equilibrium supercooled liquids", *J. Stat. Mech. Theory Exp.* **2019** (2019), article no. 064004.

[34] C. E. Maloney, A. Lemaître, "Subextensive scaling in the athermal quasistatic limit of amorphous matter in plastic shear flow", *Phys. Rev. Lett.* **93** (2004), article no. 016001.

[35] C. E. Maloney, A. Lemaître, "Amorphous systems in athermal, quasistatic shear", *Phys. Rev. E* **74** (2006), article no. 016118.

[36] M. Tsamados, A. Tanguy, C. Goldenberg, J.-L. Barrat, "Local elasticity map and plasticity in a model Lennard-Jones glass", *Phys. Rev. E* **80** (2009), article no. 026112.

[37] D. Vandembroucq, S. Roux, "Mechanical noise dependent Aging and Shear-Banding behavior in a mesoscopic model of amorphous plasticity", *Phys. Rev. B* **84** (2011), article no. 134210.

[38] M. Talamali, V. Petäjä, D. Vandembroucq, S. Roux, "Strain localization and anisotropic correlations in a mesoscopic model of amorphous plasticity", *C. R. Mécanique* **340** (2012), p. 275-288.

[39] B. Tyukodi, D. Vandembroucq, C. E. Maloney, "Diffusion in Mesoscopic Lattice Models of Amorphous Plasticity", *Phys. Rev. Lett.* **121** (2018), article no. 145501.

[40] J. D. Eshelby, "The Determination of the Elastic Field of an Ellipsoidal Inclusion, and Related Problems", *Proc. R. Soc. Lond., Ser. A* **241** (1957), no. 1226, p. 376.

[41] B. Tyukodi, S. Patinet, S. Roux, D. Vandembroucq, "From depinning transition to plastic yielding of amorphous media: A soft modes perspective", *Phys. Rev. E* **93** (2016), article no. 063005.

[42] F. Varnik, L. Bocquet, J.-L. Barrat, L. Berthier, "Shear Localization in a model glass", *Phys. Rev. Lett.* **90** (2003), article no. 095702.

[43] F. Varnik, L. Bocquet, J.-L. Barrat, "A study of the static yield stress in a binary Lennard-Jones glass", *J. Chem. Phys.* **120** (2004), p. 2788-2801.

[44] S. Patinet, D. Vandembroucq, S. Roux, "Quantitative Prediction of Effective Toughness at Random Heterogeneous Interfaces", *Phys. Rev. Lett.* **110** (2013), article no. 165507.

[45] J.-C. Baret, D. Vandembroucq, S. Roux, "An extremal model of amorphous plasticity", *Phys. Rev. Lett.* **89** (2002), article no. 195506.

[46] Z. Budrikis, D. Fernández Castellanos, S. Sandfeld, M. Zaiser, S. Zapperi, "Universal features of amorphous plasticity", *Nat. Commun.* **8** (2017), article no. 15928.

[47] D. Rodney, C. A. Schuh, "Distribution of Thermally Activated Plastic Events in a Flowing Glass", *Phys. Rev. Lett.* **102** (2009), article no. 235503.

[48] T. Albaret, A. Tanguy, F. Boioli, D. Rodney, "Mapping between atomistic simulations and Eshelby inclusions in the shear deformation of an amorphous silicon model", *Phys. Rev. E* **93** (2016), article no. 053502.

[49] E. A. Jagla, "Different universality classes at the yielding transition of amorphous systems", *Phys. Rev. E* **96** (2017), article no. 023006.

[50] I. Fernández Aguirre, E. A. Jagla, "Critical exponents of the yielding transition of amorphous solids", *Phys. Rev. E* **98** (2018), article no. 013002.